A Tale of three papers

I. M. Navon

September 28, 2012

Florida State University, Tallahassee, Florida, USA

inavon@fsu.edu

1. Abstract
2. Impact of Prof. Hussaini
3. Optimal control of cylinder wakes via suction and blowing
4. A perfectly matched layer approach for the linearized SWE models
5. Analysis of the singular vectors of the full physics FSU Global Spectral Model

Abstract

- Three papers written in collaboration with Professor Hussaini and inspired by him are briefly discussed.
- One is in computational fluid dynamics field, namely a problem of controlling vortex shedding behind a cylinder (through suction and blowing on the cylinder surface) governed by the unsteady two-dimensional incompressible Navier - Stokes equations space discretized by finite-volume approximation with time-dependent boundary conditions.

Abstract

- Three papers written in collaboration with Professor Hussaini and inspired by him are briefly discussed.
- One is in computational fluid dynamics field, namely a problem of controlling vortex shedding behind a cylinder (through suction and blowing on the cylinder surface) governed by the unsteady two-dimensional incompressible Navier - Stokes equations space discretized by finite-volume approximation with time-dependent boundary conditions.

Abstract

- The second is a topic of applied mathematics related to the so-called perfectly matched layer (PML) as an absorbing boundary condition. The equations are obtained in this layer by splitting the shallow water equations in the coordinate directions and introducing the absorption coefficients.
- The performance of the PML as an absorbing boundary treatment is demonstrated using a commonly employed bell-shaped Gaussian initially introduced at the center of the domain.

Abstract

- The second is a topic of applied mathematics related to the so-called perfectly matched layer (PML) as an absorbing boundary condition. The equations are obtained in this layer by splitting the shallow water equations in the coordinate directions and introducing the absorption coefficients.
- The performance of the PML as an absorbing boundary treatment is demonstrated using a commonly employed bell-shaped Gaussian initially introduced at the center of the domain.

Abstract

- Finally the third paper relates to the domain of meteorology namely the analysis of singular vectors (SVs) of the Florida State University Global Spectral Model and its adjoint, which includes linearized full physics of the atmosphere.
- It is demonstrated that the physical processes, especially precipitation, fundamentally affect the leading SVs. When the SVs are coupled with the precipitation geographically, their growth rates increase substantially.

Abstract

- Finally the third paper relates to the domain of meteorology namely the analysis of singular vectors (SVs) of the Florida State University Global Spectral Model and its adjoint, which includes linearized full physics of the atmosphere.
- It is demonstrated that the physical processes, especially precipitation, fundamentally affect the leading SVs. When the SVs are coupled with the precipitation geographically, their growth rates increase substantially.

Impact of Prof. Hussaini

- The impact of Professor Hussaini on these papers and the quality of their presentation is outlined.
- Importance of precise, well-crafted and well-expressed clarity of presentation
- Choice of highly original topics of reserch
- Importance of focusing reserch on "uncrowded" research areas
- Multidisciplinarity and in-depth knowledge of research topics
- Strife to perfection- lessons from a master

Optimal control of cylinder wakes via suction and blowing

- Optimal control of cylinder wakes via suction and blowing, Zhijin Li, I. M. Navon, M. Y. Hussaini, F.-X. Le Dimet, Computers & Fluids, vol. 32, no. 2, pp. 149-171, 2003 (32 citations)
- Optimal control algorithm for controlling vortex shedding behind circular cylinder in uniform stream at Reynolds numbers exceeding $Re = 40$.
- Adequate choice of cost functional as space-time integral of some physical quantity.
- Minimization of above cost functional using DFP Quasi-Newton over a time interval longer than the vortex shedding period.
- Regularization of ill-posed cost functional using Tikhonov regularization.

Optimal control of cylinder wakes via suction and blowing

- Optimal control of cylinder wakes via suction and blowing, Zhijin Li, I. M. Navon, M. Y. Hussaini, F.-X. Le Dimet, Computers & Fluids, vol. 32, no. 2, pp. 149-171, 2003 (32 citations)
- Optimal control algorithm for controlling vortex shedding behind circular cylinder in uniform stream at Reynolds numbers exceeding $Re = 40$.
- Adequate choice of cost functional as space-time integral of some physical quantity.
- Minimization of above cost functional using DFP Quasi-Newton over a time interval longer than the vortex shedding period.
- Regularization of ill-posed cost functional using Tikhonov regularization.

Optimal control of cylinder wakes via suction and blowing

- Optimal control of cylinder wakes via suction and blowing, Zhijin Li, I. M. Navon, M. Y. Hussaini, F.-X. Le Dimet, Computers & Fluids, vol. 32, no. 2, pp. 149-171, 2003 (32 citations)
- Optimal control algorithm for controlling vortex shedding behind circular cylinder in uniform stream at Reynolds numbers exceeding $Re = 40$.
- Adequate choice of cost functional as space-time integral of some physical quantity.
- Minimization of above cost functional using DFP Quasi-Newton over a time interval longer than the vortex shedding period.
- Regularization of ill-posed cost functional using Tikhonov regularization.

Optimal control of cylinder wakes via suction and blowing

- Optimal control of cylinder wakes via suction and blowing, Zhijin Li, I. M. Navon, M. Y. Hussaini, F.-X. Le Dimet, Computers & Fluids, vol. 32, no. 2, pp. 149-171, 2003 (32 citations)
- Optimal control algorithm for controlling vortex shedding behind circular cylinder in uniform stream at Reynolds numbers exceeding $Re = 40$.
- Adequate choice of cost functional as space-time integral of some physical quantity.
- Minimization of above cost functional using DFP Quasi-Newton over a time interval longer than the vortex shedding period.
- Regularization of ill-posed cost functional using Tikhonov regularization.

Optimal control of cylinder wakes via suction and blowing

- Optimal control of cylinder wakes via suction and blowing, Zhijin Li, I. M. Navon, M. Y. Hussaini, F.-X. Le Dimet, Computers & Fluids, vol. 32, no. 2, pp. 149-171, 2003 (32 citations)
- Optimal control algorithm for controlling vortex shedding behind circular cylinder in uniform stream at Reynolds numbers exceeding $Re = 40$.
- Adequate choice of cost functional as space-time integral of some physical quantity.
- Minimization of above cost functional using DFP Quasi-Newton over a time interval longer than the vortex shedding period.
- Regularization of ill-posed cost functional using Tikhonov regularization.

Optimal control of cylinder wakes via suction and blowing

- Optimal control of cylinder wakes via suction and blowing, Zhijin Li, I. M. Navon, M. Y. Hussaini, F.-X. Le Dimet, Computers & Fluids, vol. 32, no. 2, pp. 149-171, 2003 (32 citations)
- Optimal control algorithm for controlling vortex shedding behind circular cylinder in uniform stream at Reynolds numbers exceeding $Re = 40$.
- Adequate choice of cost functional as space-time integral of some physical quantity.
- Minimization of above cost functional using DFP Quasi-Newton over a time interval longer than the vortex shedding period.
- Regularization of ill-posed cost functional using Tikhonov regularization.

Mathematical Model

- Let Ω denote the flow domain.
- The flow field is described by the velocity vector (u, v) and the scalar pressure p and is obtained by solving the following momentum and mass conservation equations (in dimensionless form)

$$\frac{\partial u}{\partial t} + \frac{\partial p}{\partial t} = \frac{1}{R_e}\left(\frac{\partial^2 u}{\partial x^2} + \frac{\partial^2 u}{\partial y^2}\right) - \frac{\partial u^2}{\partial x} - \frac{\partial uv}{\partial y} \quad \text{in } \Omega,$$

$$\frac{\partial v}{\partial t} + \frac{\partial p}{\partial y} = \frac{1}{R_e}\left(\frac{\partial^2 v}{\partial x^2} + \frac{\partial^2 v}{\partial y^2}\right) - \frac{\partial uv}{\partial x} - \frac{\partial v^2}{\partial y} \quad \text{in } \Omega,$$

$$\frac{\partial u}{\partial x} + \frac{\partial v}{\partial y} = 0 \quad \text{in } \Omega,$$

subject to the initial condition

$$(u, v)|_{t=0} = (u_0, v_0) \quad \text{in } \Omega.$$

with appropriate b.c's.

Mathematical Model

- Let Ω denote the flow domain.
- The flow field is described by the velocity vector (u, v) and the scalar pressure p and is obtained by solving the following momentum and mass conservation equations (in dimensionless form)

$$\frac{\partial u}{\partial t} + \frac{\partial p}{\partial t} = \frac{1}{R_e}\left(\frac{\partial^2 u}{\partial x^2} + \frac{\partial^2 u}{\partial y^2}\right) - \frac{\partial u^2}{\partial x} - \frac{\partial uv}{\partial y} \quad \text{in } \Omega,$$

$$\frac{\partial v}{\partial t} + \frac{\partial p}{\partial y} = \frac{1}{R_e}\left(\frac{\partial^2 v}{\partial x^2} + \frac{\partial^2 v}{\partial y^2}\right) - \frac{\partial uv}{\partial x} - \frac{\partial v^2}{\partial y} \quad \text{in } \Omega,$$

$$\frac{\partial u}{\partial x} + \frac{\partial v}{\partial y} = 0 \quad \text{in } \Omega,$$

subject to the initial condition

$$(u, v)|_{t=0} = (u_0, v_0) \quad \text{in } \Omega.$$

with appropriate b.c's.

Mathematical Model

- Let Ω denote the flow domain.
- The flow field is described by the velocity vector (u, v) and the scalar pressure p and is obtained by solving the following momentum and mass conservation equations (in dimensionless form)

$$\frac{\partial u}{\partial t} + \frac{\partial p}{\partial t} = \frac{1}{R_e}(\frac{\partial^2 u}{\partial x^2} + \frac{\partial^2 u}{\partial y^2}) - \frac{\partial u^2}{\partial x} - \frac{\partial uv}{\partial y} \quad \text{in } \Omega,$$

$$\frac{\partial v}{\partial t} + \frac{\partial p}{\partial y} = \frac{1}{R_e}(\frac{\partial^2 v}{\partial x^2} + \frac{\partial^2 v}{\partial y^2}) - \frac{\partial uv}{\partial x} - \frac{\partial v^2}{\partial y} \quad \text{in } \Omega,$$

$$\frac{\partial u}{\partial x} + \frac{\partial v}{\partial y} = 0 \quad \text{in } \Omega,$$

subject to the initial condition

$$(u, v)|_{t=0} = (u_0, v_0) \quad \text{in } \Omega.$$

with appropriate b.c's.

Mathematical Model

- We used the following notation: the cylinder diameter d, the free stream velocity U and $R_e = Ud/\nu$ is the Reynolds number.
- On the surface of the cylinder injection and suction normal to the surface are allowed.
- The injection and suction are the control parameters in the present study.

Mathematical Model

- We used the following notation: the cylinder diameter d, the free stream velocity U and $R_e = Ud/\nu$ is the Reynolds number.
- On the surface of the cylinder injection and suction normal to the surface are allowed.
- The injection and suction are the control parameters in the present study.

Mathematical Model

- We used the following notation: the cylinder diameter d, the free stream velocity U and $R_e = Ud/\nu$ is the Reynolds number.
- On the surface of the cylinder injection and suction normal to the surface are allowed.
- The injection and suction are the control parameters in the present study.

Discretization scheme

- Finite-volume discretization was used is space.
- A semi-implicit method was employed for the discretization in time, which is explicit in the convective terms and implicit in the pressure term.
- The time step is calculated as

$$\Delta t = \tau \min\left(\frac{R_e}{2}\left(\frac{1}{\Delta x^2} + \frac{1}{\Delta y^2}\right)^{-1}, \frac{\Delta x}{u_{\max}}, \frac{\Delta y}{v_{\max}}\right).$$

- The factor $\tau \in [0, 1]$ was set to 0.6.

Discretization scheme

- Finite-volume discretization was used is space.
- A semi-implicit method was employed for the discretization in time, which is explicit in the convective terms and implicit in the pressure term.
- The time step is calculated as

$$\Delta t = \tau \min(\frac{R_e}{2}(\frac{1}{\Delta x^2} + \frac{1}{\Delta y^2})^{-1}, \frac{\Delta x}{u_{\max}}, \frac{\Delta y}{v_{\max}}).$$

- The factor $\tau \in [0, 1]$ was set to 0.6.

Discretization scheme

- Finite-volume discretization was used is space.
- A semi-implicit method was employed for the discretization in time, which is explicit in the convective terms and implicit in the pressure term.
- The time step is calculated as

$$\Delta t = \tau \min\left(\frac{R_e}{2}\left(\frac{1}{\Delta x^2} + \frac{1}{\Delta y^2}\right)^{-1}, \ \frac{\Delta x}{u_{\max}}, \ \frac{\Delta y}{v_{\max}}\right).$$

- The factor $\tau \in [0, 1]$ was set to 0.6.

Discretization scheme

- Finite-volume discretization was used is space.
- A semi-implicit method was employed for the discretization in time, which is explicit in the convective terms and implicit in the pressure term.
- The time step is calculated as

$$\Delta t = \tau \min\left(\frac{R_e}{2}\left(\frac{1}{\Delta x^2} + \frac{1}{\Delta y^2}\right)^{-1}, \frac{\Delta x}{u_{\max}}, \frac{\Delta y}{v_{\max}}\right).$$

- The factor $\tau \in [0, 1]$ was set to 0.6.

Typical objective functional

- An important objective is the minimization of the drag.
- For incompressible flow it can be computed from integral of dissipation function

$$J_E = \frac{\nu}{2} \int_{t_1}^{t_2} \int_{\Omega} |(\nabla \mathbf{U}) + (\nabla \mathbf{U})^T|^2 d\Omega dt,$$

  where $\mathbf{U}$ is the velocity vector with components u and v, and ν is the kinematic viscosity of the fluid.
- We used L-BFGS and Q-N minimization methods that require only storage of a few additional vectors

Typical objective functional

- An important objective is the minimization of the drag.
- For incompressible flow it can be computed from integral of dissipation function

$$J_E = \frac{\nu}{2}\int_{t_1}^{t_2}\int_{\Omega} |(\nabla \mathbf{U}) + (\nabla \mathbf{U})^T|^2 d\Omega dt,$$

  where $\mathbf{U}$ is the velocity vector with components u and v, and ν is the kinematic viscosity of the fluid.
- We used L-BFGS and Q-N minimization methods that require only storage of a few additional vectors

Typical objective functional

- An important objective is the minimization of the drag.
- For incompressible flow it can be computed from integral of dissipation function

$$J_E = \frac{\nu}{2} \int_{t_1}^{t_2} \int_{\Omega} |(\nabla \mathbf{U}) + (\nabla \mathbf{U})^T|^2 d\Omega dt,$$

  where $\mathbf{U}$ is the velocity vector with components u and v, and ν is the kinematic viscosity of the fluid.
- We used L-BFGS and Q-N minimization methods that require only storage of a few additional vectors

Typical objective functional

- To solve a "flow - tracking" problem we denote (u_d, v_d) the desired steady laminar flow

$$J_F = \frac{1}{2}\int_{t_1}^{t_2}\int_{\Omega}(|u-u_d|^2 + |v-v_d|^2 d\Omega dt.$$

Regularized objective functional

- We employed a Tikhonov regularization

$$J_{FR} = J_F + \frac{\eta}{2}|\mathbf{y}|^2 \simeq J_F + \eta\Sigma$$

where J_F is defined in previous slide, and η is the regularization parameter (a dimensionless constant), $\mathbf{y}$ is an M-dimensional control-parameter vector (which corresponds to boundary parameters), and Σ is a stabilizing function.

Figures

- Open issues
- Controllability
- Existence of solutions
- Uniqueness of solutions

Figures

- Open issues
- Controllability
- Existence of solutions
- Uniqueness of solutions

Figures

- Open issues
- Controllability
- Existence of solutions
- Uniqueness of solutions

Figures

- Open issues
- Controllability
- Existence of solutions
- Uniqueness of solutions

Figures

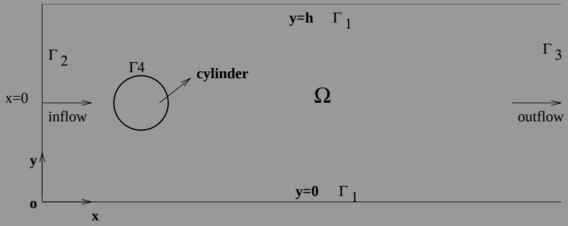

Figure 1: The geometry of the computational domain Ω. Only the left half part is shown.

Figures

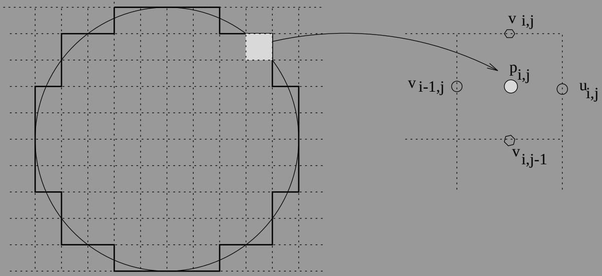

Figure 2: A schematic illustration of boundary cells and boundary values.

Figures

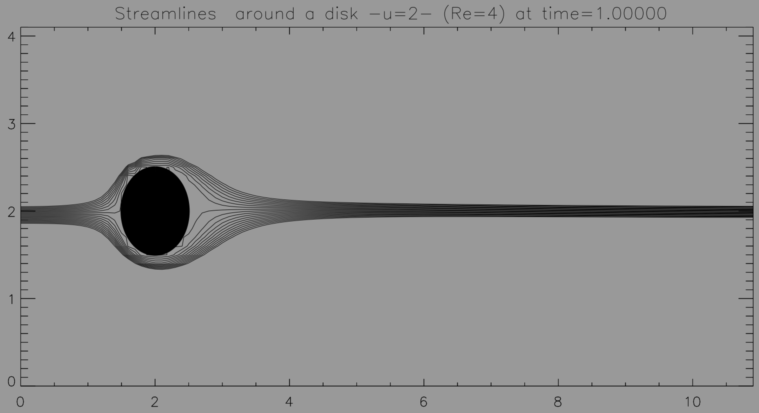

Figure 3: Streamfunction of the uncontrolled steady state for $R_e = 4.0$.

Figures

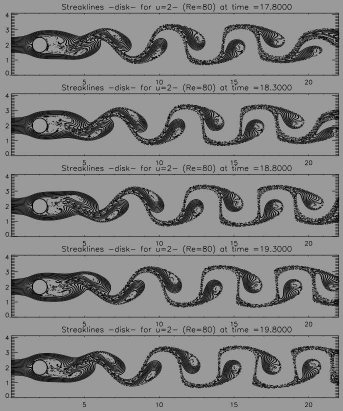

Figure 4: Evolution of streaklines during one vortex shedding period about 2.0 time units starting at the time of 17.8 time units. The Reynolds number is 80.0. The flow displays well developed Karman vortex street at the time 16.0 time units with the initial condition depicted in Fig. 3.

Figures

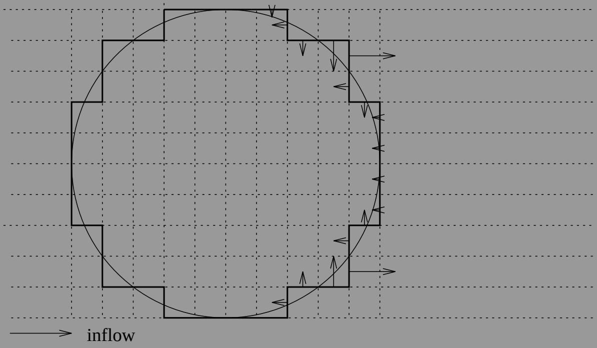

Figure 5: Distribution of optimal injection and suction for the time windows of 1.0. The optimizing flow vector is restricted to be only in the rear half of the cylinder and normal to the surface. Reynolds number is 80.0. The initial condition is the same as depicted in Fig. 4.

Figures

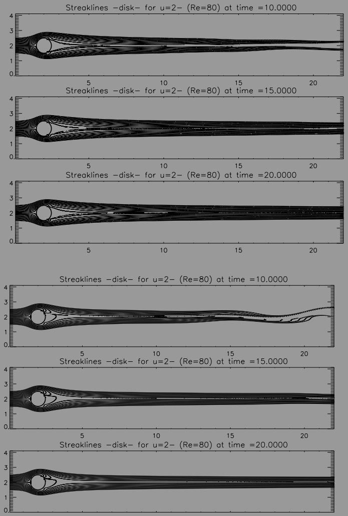

Figure 6: Evolution of streak lines for the controlled flow. The optimization time windows are 1.0 units (upper) and 3.0 units (lower).

Figures

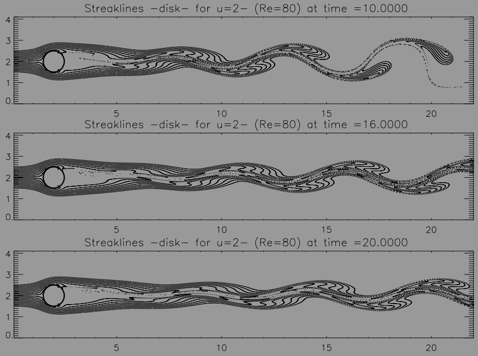

Figure 7: Evolution of streak lines for the controlled flow. The optimized injection and suction at the surface of the cylinder are obtained by minimizing J_F , with the time window starting at t = 0 with the state depicted in Fig. 4. Then the model is integrated with the initial condition at t = 20 depicted in Fig. 4.

Figures

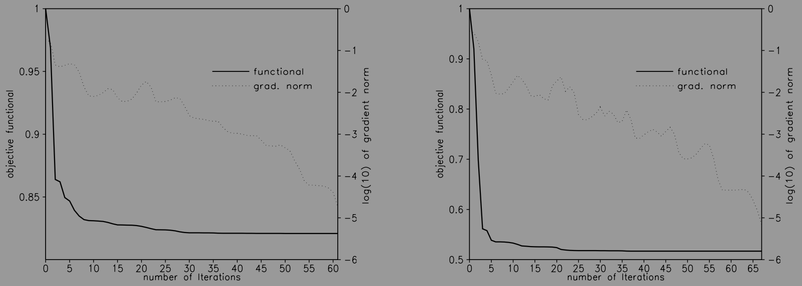

Figure 8: Evolution of both the objective functional and its gradient norm with minimization iteration numbers. The objective functional J_F is used. The time windows are 1.0 units (left) and 3.0 units (right).

Figures

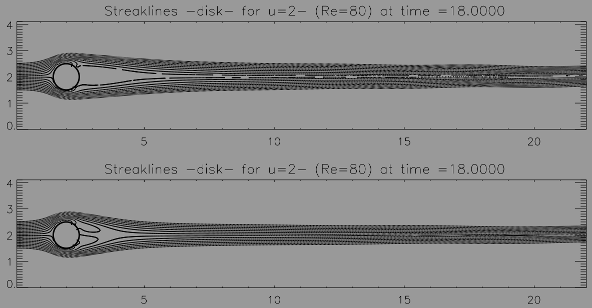

Figure 9: Steady states of streak lines of the controlled flow with the optimal injection/suction obtained after 10 minimization iterations.

Figures

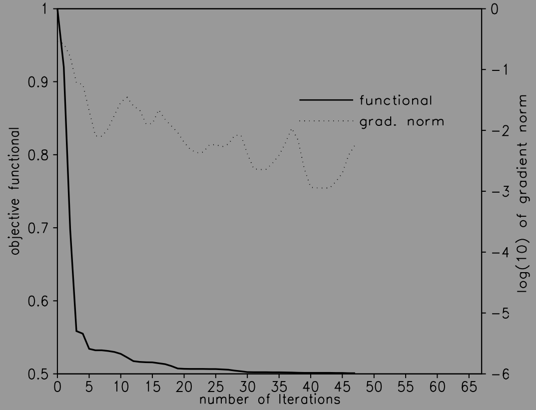

Figure 10: Same as in Fig. 8, but without regularization. The minimization stops after 47 iterations since the minimization cannot find a sufficient descent step leading to a sufficient decrease.

Conclusions

- In practical applications computing solutions of optimal control problem to full optimality is not necessary (most of the decrease achieved in first 10 iterations
- Novelty: obtaining size and location of blowing and suction on the boundary of the rear part of the cylinder
- In order to achieve robust control the time window of control (data assimilation) should be larger then the vortex shedding period, the inverse of the Strouhal frequency.

Conclusions

- In practical applications computing solutions of optimal control problem to full optimality is not necessary (most of the decrease achieved in first 10 iterations
- Novelty: obtaining size and location of blowing and suction on the boundary of the rear part of the cylinder
- In order to achieve robust control the time window of control (data assimilation) should be larger then the vortex shedding period, the inverse of the Strouhal frequency.

Conclusions

- In practical applications computing solutions of optimal control problem to full optimality is not necessary (most of the decrease achieved in first 10 iterations
- Novelty: obtaining size and location of blowing and suction on the boundary of the rear part of the cylinder
- In order to achieve robust control the time window of control (data assimilation) should be larger then the vortex shedding period, the inverse of the Strouhal frequency.

Conclusions

- In practical applications computing solutions of optimal control problem to full optimality is not necessary (most of the decrease achieved in first 10 iterations
- Novelty: obtaining size and location of blowing and suction on the boundary of the rear part of the cylinder
- In order to achieve robust control the time window of control (data assimilation) should be larger then the vortex shedding period, the inverse of the Strouhal frequency.

A perfectly matched layer approach for the linearized SWE models

- A perfectly matched layer approach to the linearized shallow water equations models, I.M. Navon, Beny Neta and M. Y. Hussaini, Monthly Weather Review , 132, No 6, 1369-1378 (2004) (43 citations)
- This topic deals with a particular application of absorbing boundary conditions called perfectly matched layer (PML) proposed by Berenger.
- The buffer/sponge layer consists in surrounding the truncated physical domain with a zone where non-physical equations are employed to damp incident waves so as to minimize reflection into physical domain of interest.
- The parameters of PML are chosen such that reflected wave amplitude is negligibly small by the time it reaches the interface between absorbing layer and interior domain.

A perfectly matched layer approach for the linearized SWE models

- A perfectly matched layer approach to the linearized shallow water equations models, I.M. Navon, Beny Neta and M. Y. Hussaini, Monthly Weather Review , 132, No 6, 1369-1378 (2004) (43 citations)
- This topic deals with a particular application of absorbing boundary conditions called perfectly matched layer (PML) proposed by Berenger.
- The buffer/sponge layer consists in surrounding the truncated physical domain with a zone where non-physical equations are employed to damp incident waves so as to minimize reflection into physical domain of interest.
- The parameters of PML are chosen such that reflected wave amplitude is negligibly small by the time it reaches the interface between absorbing layer and interior domain.

A perfectly matched layer approach for the linearized SWE models

- A perfectly matched layer approach to the linearized shallow water equations models, I.M. Navon, Beny Neta and M. Y. Hussaini, Monthly Weather Review , 132, No 6, 1369-1378 (2004) (43 citations)
- This topic deals with a particular application of absorbing boundary conditions called perfectly matched layer (PML) proposed by Berenger.
- The buffer/sponge layer consists in surrounding the truncated physical domain with a zone where non-physical equations are employed to damp incident waves so as to minimize reflection into physical domain of interest.
- The parameters of PML are chosen such that reflected wave amplitude is negligibly small by the time it reaches the interface between absorbing layer and interior domain.

A perfectly matched layer approach for the linearized SWE models

- A perfectly matched layer approach to the linearized shallow water equations models, I.M. Navon, Beny Neta and M. Y. Hussaini, Monthly Weather Review , 132, No 6, 1369-1378 (2004) (43 citations)
- This topic deals with a particular application of absorbing boundary conditions called perfectly matched layer (PML) proposed by Berenger.
- The buffer/sponge layer consists in surrounding the truncated physical domain with a zone where non-physical equations are employed to damp incident waves so as to minimize reflection into physical domain of interest.
- The parameters of PML are chosen such that reflected wave amplitude is negligibly small by the time it reaches the interface between absorbing layer and interior domain.

A perfectly matched layer approach for the linearized SWE models

- A perfectly matched layer approach to the linearized shallow water equations models, I.M. Navon, Beny Neta and M. Y. Hussaini, Monthly Weather Review , 132, No 6, 1369-1378 (2004) (43 citations)
- This topic deals with a particular application of absorbing boundary conditions called perfectly matched layer (PML) proposed by Berenger.
- The buffer/sponge layer consists in surrounding the truncated physical domain with a zone where non-physical equations are employed to damp incident waves so as to minimize reflection into physical domain of interest.
- The parameters of PML are chosen such that reflected wave amplitude is negligibly small by the time it reaches the interface between absorbing layer and interior domain.

Mathematical model

- We considered the linearized shallow water equations (SWE) on an f-plane for a rectangular domain is considered.
- We tested an advection case of a bell-shaped Gaussian propagating in parallel to the PML.
- We then proceeded to test propagation of the bell shaped Gaussian at an angle with the PML which yielded unstable solutions necessitating, as suggested by Tam et al. (1998), the use of a 9 point Laplacian filter to stabilize them.

Mathematical model

- We considered the linearized shallow water equations (SWE) on an f-plane for a rectangular domain is considered.
- We tested an advection case of a bell-shaped Gaussian propagating in parallel to the PML.
- We then proceeded to test propagation of the bell shaped Gaussian at an angle with the PML which yielded unstable solutions necessitating, as suggested by Tam et al. (1998), the use of a 9 point Laplacian filter to stabilize them.

Mathematical model

- We considered the linearized shallow water equations (SWE) on an f-plane for a rectangular domain is considered.
- We tested an advection case of a bell-shaped Gaussian propagating in parallel to the PML.
- We then proceeded to test propagation of the bell shaped Gaussian at an angle with the PML which yielded unstable solutions necessitating, as suggested by Tam et al. (1998), the use of a 9 point Laplacian filter to stabilize them.

Mathematical model

- Split-PML linearized SWE on the $f-$ plane.

$$
\begin{aligned}
&\frac{\partial u_1}{\partial t} + U\frac{\partial u}{\partial x} + \frac{\partial \phi}{\partial x} = -\sigma_x u_1, \quad \frac{\partial u_2}{\partial t} + V\frac{\partial u}{\partial y} = -\sigma_y u_2 \\
&\frac{\partial u_3}{\partial t} - fv = 0, \quad \frac{\partial v_1}{\partial t} + U\frac{\partial v}{\partial x} = -\sigma_x v_1 \\
&\frac{\partial v_2}{\partial t} + V\frac{\partial v}{\partial y} + \frac{\partial \phi}{\partial y} = -\sigma_y v_2, \quad \frac{\partial v_3}{\partial t} + fu = 0 \qquad (1) \\
&\frac{\partial \phi_1}{\partial t} + \Phi\frac{\partial u}{\partial x} + U\frac{\partial \phi}{\partial x} = -\sigma_x \phi_1 \\
&\frac{\partial \phi_2}{\partial t} + \Phi\frac{\partial v}{\partial y} + V\frac{\partial \phi}{\partial y} = -\sigma_y \phi_2
\end{aligned}
$$

Mathematical model

where

- $U = U_{mean}$, $V = V_{mean}$
- Φ is the mean geopotential height, f is the Coriolis factor
- σ_x, σ_y are the absorption coefficients in the PML.
- A dispersion relation exists between possibly complex wave vector (k_x, k_y) and possibly complex frequency

$$-\omega^2 W_x^3 W_y^3 Z \left[\Phi(X^2 + Y^2) - F^2 + Z^2\right] = 0 \qquad (2)$$

with

$$Z = 1 + iUX \qquad (3)$$

$$W_x = \sigma_x - i\omega, \; W_y = \sigma_y - i\omega \qquad (4)$$

$$X = \frac{k_x}{W_x}, \; Y = \frac{k_y}{W_y}, \; F = \frac{f}{\omega} \qquad (5)$$

Mathematical model

where

- $U = U_{mean}$, $V = V_{mean}$
- Φ is the mean geopotential height, f is the Coriolis factor
- σ_x, σ_y are the absorption coefficients in the PML.
- A dispersion relation exists between possibly complex wave vector (k_x, k_y) and possibly complex frequency

$$-\omega^2 W_x^3 W_y^3 Z \left[\Phi(X^2 + Y^2) - F^2 + Z^2\right] = 0 \tag{2}$$

with

$$Z = 1 + iUX \tag{3}$$

$$W_x = \sigma_x - i\omega, \; W_y = \sigma_y - i\omega \tag{4}$$

$$X = \frac{k_x}{W_x}, \; Y = \frac{k_y}{W_y}, \; F = \frac{f}{\omega} \tag{5}$$

Mathematical model

where

- $U = U_{mean}, V = V_{mean}$
- Φ is the mean geopotential height, f is the Coriolis factor
- $\sigma_x,\ \sigma_y$ are the absorption coefficients in the PML.
- A dispersion relation exists between possibly complex wave vector (k_x, k_y) and possibly complex frequency

$$-\omega^2 W_x^3 W_y^3 Z\left[\Phi(X^2+Y^2) - F^2 + Z^2\right] = 0 \tag{2}$$

with

$$Z = 1 + iUX \tag{3}$$

$$W_x = \sigma_x - i\omega,\ W_y = \sigma_y - i\omega \tag{4}$$

$$X = \frac{k_x}{W_x},\ Y = \frac{k_y}{W_y},\ F = \frac{f}{\omega} \tag{5}$$

Mathematical model

where

- $U = U_{mean}, V = V_{mean}$
- Φ is the mean geopotential height, f is the Coriolis factor
- $\sigma_x,\ \sigma_y$ are the absorption coefficients in the PML.
- A dispersion relation exists between possibly complex wave vector (k_x, k_y) and possibly complex frequency

$$-\omega^2 W_x^3 W_y^3 Z \left[\Phi(X^2 + Y^2) - F^2 + Z^2\right] = 0 \tag{2}$$

with

$$Z = 1 + iUX \tag{3}$$

$$W_x = \sigma_x - i\omega,\ W_y = \sigma_y - i\omega \tag{4}$$

$$X = \frac{k_x}{W_x},\ Y = \frac{k_y}{W_y},\ F = \frac{f}{\omega} \tag{5}$$

Plane Waves in a perfectly matched layer

- If we have a plane wave

$$\Psi = \Psi_0 e^{i(k_x x + k_y y - \omega t)}$$

$$\Psi = (u_1, u_2, u_3, v_1, v_2, v_3, \phi_1, \phi_2)$$

is the solution of PML system if

1. Triplet (w, k_x, k_y) satisfies dispersion equation.
2. Amplitudes of Φ_0 are solution of the linear homogeneous system for which the determinant is the dispersion equation.
3. Perfect transmission sufficient condition is

$$\sigma_{y_1} = \sigma_{y_2}.$$

Plane Waves in a perfectly matched layer

- If we have a plane wave

$$\Psi = \Psi_0 e^{i(k_x x + k_y y - \omega t)}$$

$$\Psi = (u_1, u_2, u_3, v_1, v_2, v_3, \phi_1, \phi_2)$$

is the solution of PML system if

1. Triplet (w, k_x, k_y) satisfies dispersion equation.
2. Amplitudes of Φ_0 are solution of the linear homogeneous system for which the determinant is the dispersion equation.
3. Perfect transmission sufficient condition is

$$\sigma_{y_1} = \sigma_{y_2}.$$

Plane Waves in a perfectly matched layer

- If we have a plane wave

$$\Psi = \Psi_0 e^{i(k_x x + k_y y - \omega t)}$$

$$\Psi = (u_1, u_2, u_3, v_1, v_2, v_3, \phi_1, \phi_2)$$

is the solution of PML system if

1. Triplet (w, k_x, k_y) satisfies dispersion equation.
2. Amplitudes of Φ_0 are solution of the linear homogeneous system for which the determinant is the dispersion equation.
3. Perfect transmission sufficient condition is

$$\sigma_{y_1} = \sigma_{y_2}.$$

Plane Waves in a perfectly matched layer

- If we have a plane wave

$$\Psi = \Psi_0 e^{i(k_x x + k_y y - \omega t)}$$

$$\Psi = (u_1, u_2, u_3, v_1, v_2, v_3, \phi_1, \phi_2)$$

is the solution of PML system if

1. Triplet (w, k_x, k_y) satisfies dispersion equation.
2. Amplitudes of Φ_0 are solution of the linear homogeneous system for which the determinant is the dispersion equation.
3. Perfect transmission sufficient condition is

$$\sigma_{y_1} = \sigma_{y_2}.$$

Numerical testing

- This scheme is implemented on a non-staggered grid
- The scheme has a CFL stability condition

$$\Delta t \leq \frac{\sqrt{(\Delta x)^2 + (\Delta y)^2}}{\sqrt{\Phi}\sqrt{2}}$$

- Spatial differencing of the linearized shallow water equations was carried out on a rectangular domain of 141×141 grid points
- uniform spatial horizontal grid length of $\Delta x = \Delta y = 100km$.
- We used $H = h_{av} = 5000m$ and a time step of $\Delta t = 120sec$.

Numerical testing

- This scheme is implemented on a non-staggered grid
- The scheme has a CFL stability condition

$$\Delta t \leq \frac{\sqrt{(\Delta x)^2 + (\Delta y)^2}}{\sqrt{\Phi}\sqrt{2}}$$

- Spatial differencing of the linearized shallow water equations was carried out on a rectangular domain of 141×141 grid points
- uniform spatial horizontal grid length of $\Delta x = \Delta y = 100km$.
- We used $H = h_{av} = 5000m$ and a time step of $\Delta t = 120sec$.

Numerical testing

- This scheme is implemented on a non-staggered grid
- The scheme has a CFL stability condition

$$\Delta t \leq \frac{\sqrt{(\Delta x)^2 + (\Delta y)^2}}{\sqrt{\Phi}\sqrt{2}}$$

- Spatial differencing of the linearized shallow water equations was carried out on a rectangular domain of 141×141 grid points
- uniform spatial horizontal grid length of $\Delta x = \Delta y = 100km$.
- We used $H = h_{av} = 5000m$ and a time step of $\Delta t = 120sec$.

Numerical testing

- This scheme is implemented on a non-staggered grid
- The scheme has a CFL stability condition

$$\Delta t \leq \frac{\sqrt{(\Delta x)^2 + (\Delta y)^2}}{\sqrt{\Phi}\sqrt{2}}$$

- Spatial differencing of the linearized shallow water equations was carried out on a rectangular domain of 141×141 grid points
- uniform spatial horizontal grid length of $\Delta x = \Delta y = 100km$.
- We used $H = h_{av} = 5000m$ and a time step of $\Delta t = 120sec$.

Numerical testing

- This scheme is implemented on a non-staggered grid
- The scheme has a CFL stability condition

$$\Delta t \leq \frac{\sqrt{(\Delta x)^2 + (\Delta y)^2}}{\sqrt{\Phi}\sqrt{2}}$$

- Spatial differencing of the linearized shallow water equations was carried out on a rectangular domain of 141×141 grid points
- uniform spatial horizontal grid length of $\Delta x = \Delta y = 100km$.
- We used $H = h_{av} = 5000m$ and a time step of $\Delta t = 120sec$.

Numerical testing

- We compared the results with a control simulation computed on a much larger domain of 400×400 grid points unaffected by b.c. for the integration time-span.
- The experiment starts with a bell-shaped Gaussian at the center of the domain

$$\phi(x,y,0) = \phi_0 + \hat{\phi} \exp\left\{-\left[\frac{x-L_x/2}{L_x/10}\right]^2\right\} \exp\left\{-\left[\frac{y-L_y/2}{L_y/10}\right]^2\right\} \quad (6)$$

- $L_x = L_y = 10,000km$, $\phi_0 = (5000m)\cdot g$, and $\hat{\phi} = (500m)\cdot g$.

Numerical testing

- We compared the results with a control simulation computed on a much larger domain of 400×400 grid points unaffected by b.c. for the integration time-span.
- The experiment starts with a bell-shaped Gaussian at the center of the domain

$$\phi(x,y,0) = \phi_0 + \hat{\phi}\exp\left\{-\left[\frac{x-L_x/2}{L_x/10}\right]^2\right\}\exp\left\{-\left[\frac{y-L_y/2}{L_y/10}\right]^2\right\} \quad (6)$$

- $L_x = L_y = 10,000km$, $\phi_0 = (5000m)\cdot g$, and $\hat{\phi} = (500m)\cdot g$.

Numerical testing

- We compared the results with a control simulation computed on a much larger domain of 400×400 grid points unaffected by b.c. for the integration time-span.
- The experiment starts with a bell-shaped Gaussian at the center of the domain

$$\phi(x,y,0) = \phi_0 + \hat{\phi} \exp\left\{-\left[\frac{x - L_x/2}{L_x/10}\right]^2\right\} \exp\left\{-\left[\frac{y - L_y/2}{L_y/10}\right]^2\right\} \tag{6}$$

- $L_x = L_y = 10,000km$, $\phi_0 = (5000m) \cdot g$, and $\hat{\phi} = (500m) \cdot g$.

Numerical testing

- The PML absorption coefficients varied gradually inside the PML

$$\sigma_x = \sigma_m \left| \frac{x - x_l}{D} \right|^\gamma, \ \sigma_y = \sigma_m \left| \frac{y - y_l}{D} \right|^\gamma,$$

- x_l, y_l denotes location where the PML starts, D is the depth of the PML layer.
- γ is a constant.
- The PML depth was $20\Delta x$, and the parameters governing the spatial variation of σ for the absorbing layer were $\gamma = 3$ and

$$\sigma_m = \sigma_x = \sigma_y = 0.0018.$$

Numerical testing

- The PML absorption coefficients varied gradually inside the PML
$$\sigma_x = \sigma_m \left| \frac{x - x_l}{D} \right|^\gamma, \ \sigma_y = \sigma_m \left| \frac{y - y_l}{D} \right|^\gamma,$$
- x_l, y_l denotes location where the PML starts, D is the depth of the PML layer.
- γ is a constant.
- The PML depth was $20\Delta x$, and the parameters governing the spatial variation of σ for the absorbing layer were $\gamma = 3$ and
$$\sigma_m = \sigma_x = \sigma_y = 0.0018.$$

Numerical testing

- The PML absorption coefficients varied gradually inside the PML
$$\sigma_x = \sigma_m \left| \frac{x - x_l}{D} \right|^\gamma, \ \sigma_y = \sigma_m \left| \frac{y - y_l}{D} \right|^\gamma,$$
- x_l, y_l denotes location where the PML starts, D is the depth of the PML layer.
- γ is a constant.
- The PML depth was $20\Delta x$, and the parameters governing the spatial variation of σ for the absorbing layer were $\gamma = 3$ and
$$\sigma_m = \sigma_x = \sigma_y = 0.0018.$$

Test1

- Propagation parallel to the PML axis. Mean Absolute Divergence should be zero.
- Without PML divergence shows a drastic increase as the bell reaches the boundary.
- With PML or with very large computational domain the results tend to non-divergence as mandated by the analytical solution.

Test1

- Propagation parallel to the PML axis. Mean Absolute Divergence should be zero.
- Without PML divergence shows a drastic increase as the bell reaches the boundary.
- With PML or with very large computational domain the results tend to non-divergence as mandated by the analytical solution.

Test1

- Propagation parallel to the PML axis. Mean Absolute Divergence should be zero.
- Without PML divergence shows a drastic increase as the bell reaches the boundary.
- With PML or with very large computational domain the results tend to non-divergence as mandated by the analytical solution.

Test2

- Propagation at an angle of 45° exiting through a corner.
- Here the σ curve follows a cubic spline until the full value of $\sigma_x = \sigma_y = \sigma_m$ is attained.
- Here PML excites unstable solution.
- Controlled by a 9 point Laplacian.

Test2

- Propagation at an angle of 45° exiting through a corner.
- Here the σ curve follows a cubic spline until the full value of $\sigma_x = \sigma_y = \sigma_m$ is attained.
- Here PML excites unstable solution.
- Controlled by a 9 point Laplacian.

Test2

- Propagation at an angle of 45° exiting through a corner.
- Here the σ curve follows a cubic spline until the full value of $\sigma_x = \sigma_y = \sigma_m$ is attained.
- Here PML excites unstable solution.
- Controlled by a 9 point Laplacian.

Test2

- Propagation at an angle of 45° exiting through a corner.
- Here the σ curve follows a cubic spline until the full value of $\sigma_x = \sigma_y = \sigma_m$ is attained.
- Here PML excites unstable solution.
- Controlled by a 9 point Laplacian.

Figures

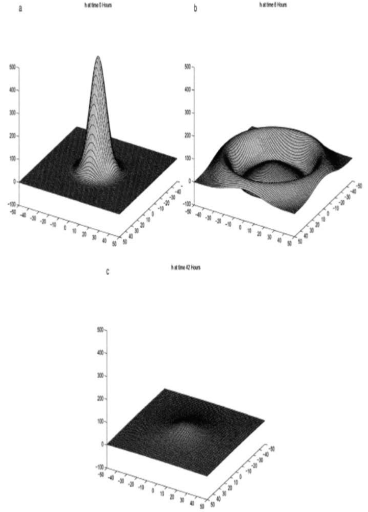

FIG. 1. The adjustment of a bell shape using PML absorbing boundary condition at (a) 0 h, (b) 6-h forecast, and (c) 42-h forecast.

Figures

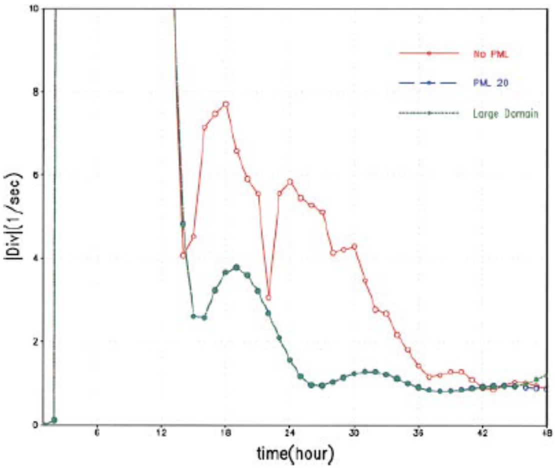

FIG. 2. Graph of the mean absolute divergence (s^{-1}) for the adjustment case multiplied by 10^8. Case of no PML, large computational domain, and a PML of 20-gridpoint thickness are displayed (in red, green, and blue, respectively).

Figures

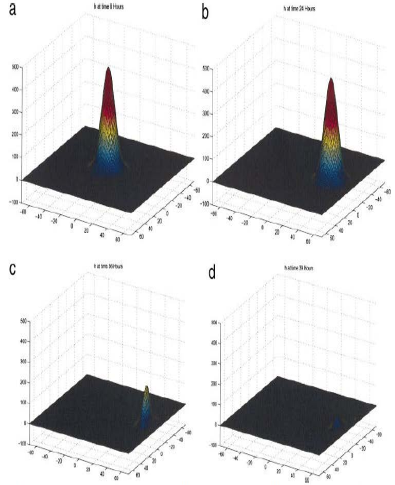

FIG. 3. The advection of a bell shape out of the computational domain moving parallel to PML x direction at (a) 0 h, (b) 24-h forecast, (c) 36-h forecast, and (d) 39-h forecast.

Figures

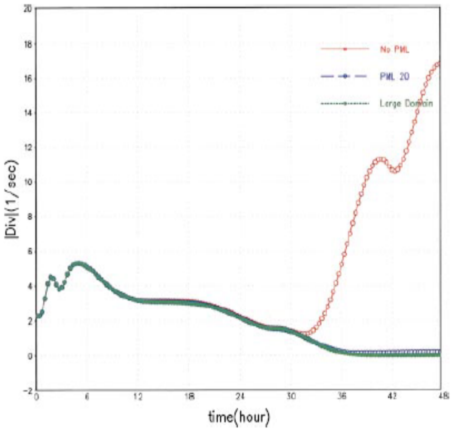

FIG. 4. Graph of the mean absolute divergence (s^{-1}) for the case of advection of a bell shape out of the computational domain moving parallel to PML multiplied by 10^8. Case of no PML, large computational domain, and a PML of 20-gridpoint thickness are displayed (in red, green, and blue, respectively).

Figures

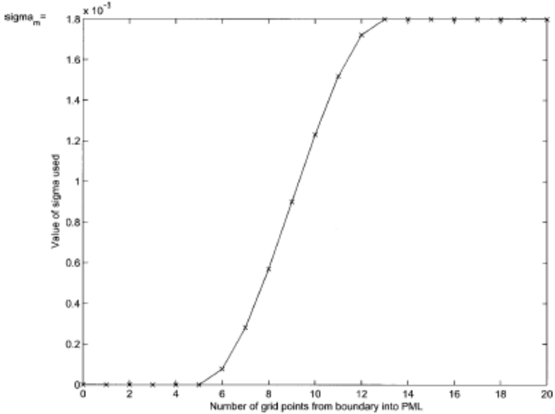

FIG. 5. Distribution of sigma within the PML layer for the case of bell propagation at an angle of 45°.

Figures

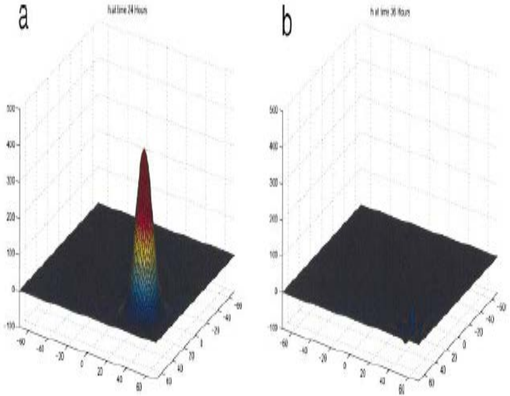

FIG. 6. The advection of a bell shape out of the computational domain moving at angle of 45° to PML x direction at (a) 24-h and (b) 36-h forecast.

Figures

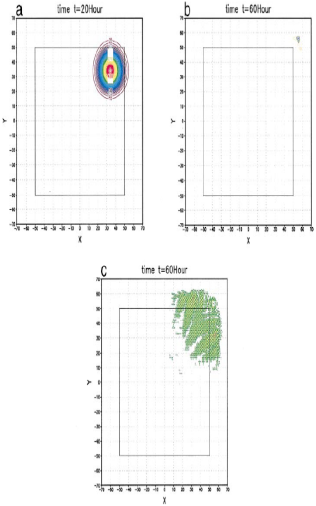

Fig. 7. The advection of the bell shape (2D) out of the computational domain moving at an angle of 45° to PML at (a) 20-h and (b) 60-h forecast using a 9 point filter. Simulation showing damping of unstable waves. (c) At 60-hour forecast without using the 9 point filter. Simulation showing propagation of unstable waves in the PML.

Figures

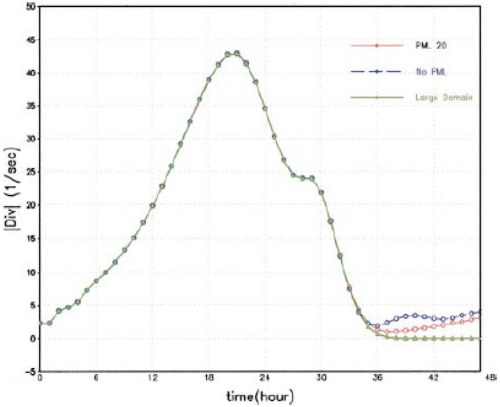

FIG. 8. Graph of the mean absolute divergence (s^{-1}) for the case of advection of a bell shape out of the computational domain moving at an angle of 45° to PML multiplied by 10^8. Case of no PML, large computational domain, and a PML of 20-gridpoint thickness are displayed (in red, green, and blue, respectively).

Novelty

- PML may improve b.c. for meso-scale models that use combination of nudging and sponge layer approaches.
- Gravity wave can both leave the domain or enter it without hindrance.
- Generalization to full 3D NWP models using normal mode decomposition yielding a shallow water equation for each vertical mode with different equivalent depth.

Novelty

- PML may improve b.c. for meso-scale models that use combination of nudging and sponge layer approaches.
- Gravity wave can both leave the domain or enter it without hindrance.
- Generalization to full 3D NWP models using normal mode decomposition yielding a shallow water equation for each vertical mode with different equivalent depth.

Novelty

- PML may improve b.c. for meso-scale models that use combination of nudging and sponge layer approaches.
- Gravity wave can both leave the domain or enter it without hindrance.
- Generalization to full 3D NWP models using normal mode decomposition yielding a shallow water equation for each vertical mode with different equivalent depth.

Analysis of the singular vectors of the full physics FSU Global Spectral Model

- Analysis of the singular vectors of the full-physics Florida State University Global Spectral Model, Zhijin Li, I.M. Navon and M. Y. Hussaini, Tellus , Vol. 57A , 560-574 (2005) (12 citations)
- FSUGSM (Krishnamurti et al. 1991) is the result of work of several decades by group of Prof. T.N. Krishnamurti.
- Its adjoint model was derived by Wang and Navon 1993, Tsuyuki 1996, Zhu and Navon 1997-1999, Li et al. 2000.

Analysis of the singular vectors of the full physics FSU Global Spectral Model

- Analysis of the singular vectors of the full-physics Florida State University Global Spectral Model, Zhijin Li, I.M. Navon and M. Y. Hussaini, Tellus , Vol. 57A , 560-574 (2005) (12 citations)
- FSUGSM (Krishnamurti et al. 1991) is the result of work of several decades by group of Prof. T.N. Krishnamurti.
- Its adjoint model was derived by Wang and Navon 1993, Tsuyuki 1996, Zhu and Navon 1997-1999, Li et al. 2000.

Analysis of the singular vectors of the full physics FSU Global Spectral Model

- Analysis of the singular vectors of the full-physics Florida State University Global Spectral Model, Zhijin Li, I.M. Navon and M. Y. Hussaini, Tellus , Vol. 57A , 560-574 (2005) (12 citations)
- FSUGSM (Krishnamurti et al. 1991) is the result of work of several decades by group of Prof. T.N. Krishnamurti.
- Its adjoint model was derived by Wang and Navon 1993, Tsuyuki 1996, Zhu and Navon 1997-1999, Li et al. 2000.

Analysis of the singular vectors of the full physics FSU Global Spectral Model

- Analysis of the singular vectors of the full-physics Florida State University Global Spectral Model, Zhijin Li, I.M. Navon and M. Y. Hussaini, Tellus , Vol. 57A , 560-574 (2005) (12 citations)
- FSUGSM (Krishnamurti et al. 1991) is the result of work of several decades by group of Prof. T.N. Krishnamurti.
- Its adjoint model was derived by Wang and Navon 1993, Tsuyuki 1996, Zhu and Navon 1997-1999, Li et al. 2000.

Singular value decomposition

- Consider the FSUGSM, which is perturbed at any point in its nonlinear trajectory.
- The evolution of the perturbation state vector x is then governed by

$$x_t = A(t,0)x_0, \qquad (7)$$

- x_t is the perturbation at time t, x_0 is the initial perturbation at time 0
- $A(t,0)$ is the linearized version of nonlinear model i.e. the tangent linear model.
- the perturbation state vector x represents $\{u, v, T, \ln \pi\}$, which are the perturbations of velocity components, temperature, and logarithm of surface pressure respectively.

Singular value decomposition

- Consider the FSUGSM, which is perturbed at any point in its nonlinear trajectory.
- The evolution of the perturbation state vector x is then governed by

$$x_t = A(t,0)x_0, \tag{7}$$

- x_t is the perturbation at time t, x_0 is the initial perturbation at time 0
- $A(t,0)$ is the linearized version of nonlinear model i.e. the tangent linear model.
- the perturbation state vector x represents $\{u, v, T, \ln\pi\}$, which are the perturbations of velocity components, temperature, and logarithm of surface pressure respectively.

Singular value decomposition

- Consider the FSUGSM, which is perturbed at any point in its nonlinear trajectory.
- The evolution of the perturbation state vector x is then governed by

$$x_t = A(t,0)x_0, \tag{7}$$

- x_t is the perturbation at time t, x_0 is the initial perturbation at time 0
- $A(t,0)$ is the linearized version of nonlinear model i.e. the tangent linear model.
- the perturbation state vector x represents $\{u, v, T, \ln\pi\}$, which are the perturbations of velocity components, temperature, and logarithm of surface pressure respectively.

Singular value decomposition

- Consider the FSUGSM, which is perturbed at any point in its nonlinear trajectory.
- The evolution of the perturbation state vector x is then governed by

$$x_t = A(t,0)x_0, \tag{7}$$

- x_t is the perturbation at time t, x_0 is the initial perturbation at time 0
- $A(t,0)$ is the linearized version of nonlinear model i.e. the tangent linear model.
- the perturbation state vector x represents $\{u, v, T, \ln \pi\}$, which are the perturbations of velocity components, temperature, and logarithm of surface pressure respectively.

Singular value decomposition

- In order to compute the fastest growing perturbations (the so-called singular vectors that will be defined precisely later), it is necessary to define an inner product for the linear vector space of perturbations.
- We introduce the dry total energy norm

$$||x||^2 = (x,x) =< x, Ex >= \frac{1}{2}\int_0^1 \int_\Sigma \left[u^2 + v^2 + \frac{c_p}{T_r}T^2\right](\frac{\partial p}{\partial \sigma})d\Sigma d\sigma +$$

$$\frac{1}{2}\int_\Sigma R_d T_r P_r (ln\pi)^2 d\Sigma.$$

- C_p is the specific heat of dry air at constant pressure, R_d the gas constant for dry air,
- $T_r = 300K$ a reference temperature, $P_r = 800hpa$ a reference pressure.
- E is a positive-definite diagonal matrix.

Singular value decomposition

- In order to compute the fastest growing perturbations (the so-called singular vectors that will be defined precisely later), it is necessary to define an inner product for the linear vector space of perturbations.
- We introduce the dry total energy norm

$$||x||^2 = (x,x) =< x, Ex >= \frac{1}{2}\int_0^1 \int_\Sigma \left[u^2 + v^2 + \frac{c_p}{T_r}T^2\right] (\frac{\partial p}{\partial \sigma}) d\Sigma d\sigma +$$

$$\frac{1}{2}\int_\Sigma R_d T_r P_r (ln\pi)^2 d\Sigma.$$

- C_p is the specific heat of dry air at constant pressure, R_d the gas constant for dry air,
- $T_r = 300K$ a reference temperature, $P_r = 800hpa$ a reference pressure.
- E is a positive-definite diagonal matrix.

Singular value decomposition

- In order to compute the fastest growing perturbations (the so-called singular vectors that will be defined precisely later), it is necessary to define an inner product for the linear vector space of perturbations.
- We introduce the dry total energy norm

$$||x||^2 = (x, x) =< x, Ex >= \frac{1}{2}\int_0^1 \int_\Sigma \left[u^2 + v^2 + \frac{c_p}{T_r}T^2\right] (\frac{\partial p}{\partial \sigma}) d\Sigma d\sigma +$$

$$\frac{1}{2}\int_\Sigma R_d T_r P_r (ln\pi)^2 d\Sigma.$$

- C_p is the specific heat of dry air at constant pressure, R_d the gas constant for dry air,
- $T_r = 300K$ a reference temperature, $P_r = 800hpa$ a reference pressure.
- E is a positive-definite diagonal matrix.

Singular value decomposition

- In order to compute the fastest growing perturbations (the so-called singular vectors that will be defined precisely later), it is necessary to define an inner product for the linear vector space of perturbations.
- We introduce the dry total energy norm

$$||x||^2 = (x,x) =< x, Ex >= \frac{1}{2}\int_0^1 \int_\Sigma \left[u^2 + v^2 + \frac{c_p}{T_r}T^2\right](\frac{\partial p}{\partial \sigma})d\Sigma d\sigma +$$

$$\frac{1}{2}\int_\Sigma R_d T_r P_r (ln\pi)^2 d\Sigma.$$

- C_p is the specific heat of dry air at constant pressure, R_d the gas constant for dry air,
- $T_r = 300K$ a reference temperature, $P_r = 800hpa$ a reference pressure.
- E is a positive-definite diagonal matrix.

Singular value decomposition

- The definition of the norm allows one to relate the energy of the perturbation x at time t to its initial value

$$\frac{||x_t||^2}{||x_0||^2} = \frac{< x_t, E_t x_t >}{< x_0, E_0 x_0 >} = \frac{< Ax_0, E_t A x_0 >}{< x_0, E_0 x_0 >} = \frac{< x_0, A^T E_t A x_0 >}{< x_0, E_0 x_0 >} = \lambda^2, \tag{8}$$

- Superscript T represents the transpose, and the subscripts t and 0 denote the weight matrix at time t and 0.
- $E_t = E_0$ and λ is usually called the energy amplification factor.

Singular value decomposition

- The definition of the norm allows one to relate the energy of the perturbation x at time t to its initial value

$$\frac{||x_t||^2}{||x_0||^2} = \frac{< x_t, E_t x_t >}{< x_0, E_0 x_0 >} = \frac{< Ax_0, E_t Ax_0 >}{< x_0, E_0 x_0 >} = \frac{< x_0, A^T E_t Ax_0 >}{< x_0, E_0 x_0 >} = \lambda^2, \tag{8}$$

- Superscript T represents the transpose, and the subscripts t and 0 denote the weight matrix at time t and 0.
- $E_t = E_0$ and λ is usually called the energy amplification factor.

Singular value decomposition

- The definition of the norm allows one to relate the energy of the perturbation x at time t to its initial value

$$\frac{||x_t||^2}{||x_0||^2} = \frac{< x_t, E_t x_t >}{< x_0, E_0 x_0 >} = \frac{< A x_0, E_t A x_0 >}{< x_0, E_0 x_0 >} = \frac{< x_0, A^T E_t A x_0 >}{< x_0, E_0 x_0 >} = \lambda^2, \tag{8}$$

- Superscript T represents the transpose, and the subscripts t and 0 denote the weight matrix at time t and 0.
- $E_t = E_0$ and λ is usually called the energy amplification factor.

Singular value decomposition

- We obtain the generalized eigenvalue problem,

$$A^T E_t A v_i = \lambda_i^2 E_0 v_i. \tag{9}$$

- The generalized eigenvectors v_i and the generalized eigenvalues λ_i are the singular vectors and singular values of A w.r.t. E_0-norm

Singular value decomposition

- We obtain the generalized eigenvalue problem,

$$A^T E_t A v_i = \lambda_i^2 E_0 v_i. \tag{9}$$

- The generalized eigenvectors v_i and the generalized eigenvalues λ_i are the singular vectors and singular values of A w.r.t. E_0-norm

Singular value decomposition

- In practice, one can only compute a small number of singular vectors compared with the huge dimension of the model variables.
- In order to make the singular vectors more relevant to limited area models, Barkmeijer (1992) introduced a local projection operator P, which sets model variables to zero outside the concerned area.
- The definition of the amplification factor is generalized as

$$\lambda^2 = \frac{< Px_t, E_t Px_t >}{< x_0, E_0 x_0 >}. \tag{10}$$

Singular value decomposition

- In practice, one can only compute a small number of singular vectors compared with the huge dimension of the model variables.
- In order to make the singular vectors more relevant to limited area models, Barkmeijer (1992) introduced a local projection operator P, which sets model variables to zero outside the concerned area.
- The definition of the amplification factor is generalized as

$$\lambda^2 = \frac{< Px_t, E_t P x_t >}{< x_0, E_0 x_0 >}. \tag{10}$$

Singular value decomposition

- In practice, one can only compute a small number of singular vectors compared with the huge dimension of the model variables.
- In order to make the singular vectors more relevant to limited area models, Barkmeijer (1992) introduced a local projection operator P, which sets model variables to zero outside the concerned area.
- The definition of the amplification factor is generalized as

$$\lambda^2 = \frac{< Px_t, E_t P x_t >}{< x_0, E_0 x_0 >}. \tag{10}$$

Numerical tests

- Test of model without physics
- Test of model with boundary layer physics.
- A measure of similarity based on projection of a set of SVs on another is provided by the similarity index of the two cases NP and BP and is defined as:

$$s(A,B;N) = \frac{1}{N}\sum_{i,j=1}^{N} m_{i,j}(A,B),$$

$$m_{ij}(NP,BP) = (< v_i(NP); Ev_j(BP) >)^2.$$

- Test with a model with "full physics"

Numerical tests

- Test of model without physics
- Test of model with boundary layer physics.
- A measure of similarity based on projection of a set of SVs on another is provided by the similarity index of the two cases NP and BP and is defined as:

$$s(A,B;N) = \frac{1}{N}\sum_{i,j=1}^{N} m_{i,j}(A,B),$$

$$m_{ij}(NP,BP) = (< v_i(NP); Ev_j(BP) >)^2.$$

- Test with a model with "full physics"

Numerical tests

- Test of model without physics
- Test of model with boundary layer physics.
- A measure of similarity based on projection of a set of SVs on another is provided by the similarity index of the two cases NP and BP and is defined as:

$$s(A,B;N) = \frac{1}{N} \sum_{i,j=1}^{N} m_{i,j}(A,B),$$

$$m_{ij}(NP,BP) = (< v_i(NP); Ev_j(BP) >)^2.$$

- Test with a model with "full physics"

Numerical tests

- Test of model without physics
- Test of model with boundary layer physics.
- A measure of similarity based on projection of a set of SVs on another is provided by the similarity index of the two cases NP and BP and is defined as:

$$s(A,B;N) = \frac{1}{N} \sum_{i,j=1}^{N} m_{i,j}(A,B),$$

$$m_{ij}(NP,BP) = (< v_i(NP); Ev_j(BP) >)^2.$$

- Test with a model with "full physics"

Conclusions

- Precipitation effects leading SV only when it is the SV perturbation geographically coupled with the precipitation process.
- Impact of filtering technique

Figures

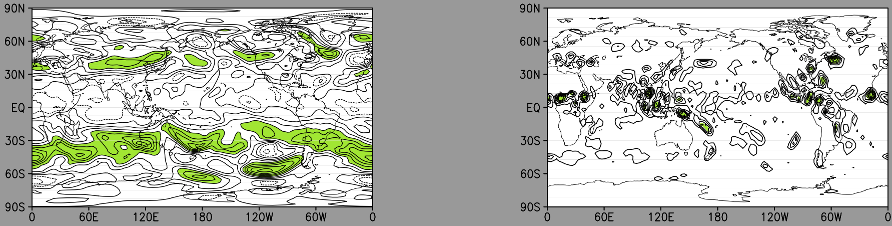

Figure 11: (a) Zonal wind analysis at 300 hPa and valid at 00 UTC 3 September 1996. The contour interval is 10.0 m, and negative values are dashed and values larger than 30.0 m shaded. (b) Accumulated precipitation of the forecast over 36 h. The contour interval is 10.0 mm, and values larger than 30.0 mm are shaded.

Figures